Pergamon

Int. J. Heat Mass Transfer. Vol. 39, No. 1, pp. 49–59, 1996

0017-9310/96 $9.50+0.00

0017-9310(95)00115-8

Conjugate natural convection in a planar thermosyphon with multiple inlets—I. Velocity and temperature fields

JOHN FLEMING and M. RUHUL AMIN†

Department of Mechanical Engineering, Montana State University, Bozeman, MT 59717, U.S.A.

(*Received* 18 *May* 1994 *and in final form* 24 *February* 1995)

Abstract—A numerical investigation of flow ($Pr = 0.71$) and temperature fields in a planar open loop thermosyphon is presented. The thermosyphon flow path is a modified 'U' shape with an upper and lower inlet in the right channel of the 'U'. The flow was studied for different values of the governing parameters. These include the Rayleigh number (Ra), the lower inlet width and the wall thermal conductivity. Results indicate the temperature field is independent of the inlet configuration at large Ra. The flow field is highly dependent on the lower inlet as recirculation at the outlet increases with inlet restrictions and boundary layer development at the heated wall. The wall thermal conductivity has large effects due to conduction resistance of the conducting walls and reduced natural convection effects.

1. INTRODUCTION

The thermosyphon is a natural convection heat transfer device or configuration which makes use of thermal buoyancy forces to drive fluid circulation in systems that may be closed, partially open, or fully open. Of interest here is the open loop thermosyphon in which a circulating fluid is exchanged with a large external (nearly) constant temperature reservoir. A typical open loop thermosyphon forms a 'U' shaped flow path.

Open loop thermosyphons have been successfully applied in a number of ways. As shown by Clarksean [1], passive heat removal from stored nuclear materials is an area of recent interest. The U.S. advanced liquid metal reactor (ALMR) design utilizes the open loop configuration to achieve inherently safe heat removal from a nuclear reactor in the event of the loss of primary coolant [2]. On a much larger scale, Torrance [3] modelled geothermal processes as open loop thermosyphons.

The objective of the present study is to conduct a steady state numerical investigation of a single phase open loop thermosyphon. The geometry of the problem considered here is shown in Fig. 1. Linear dimensions in Fig. 1 are shown in lower case, while the corresponding normalized dimensions are in upper case and enclosed in parentheses. All linear dimensions are normalized with respect to the inner channel width $b(B = 1)$.

A Newtonian fluid (air, $Pr = 0.71$) flows in the planar thermosyphon and is exchanged with constant temperature (T_∞) surroundings. A left wall and partition wall of the same material and finite thermal conductivity along with the right wall form the inner and outer channels. Fluid may enter the thermosyphon at two inlets placed at the upper and lower extremities of the outer channel. Fluid exits to the surroundings from the top of the inner channel. The flow is driven by a constant temperature boundary

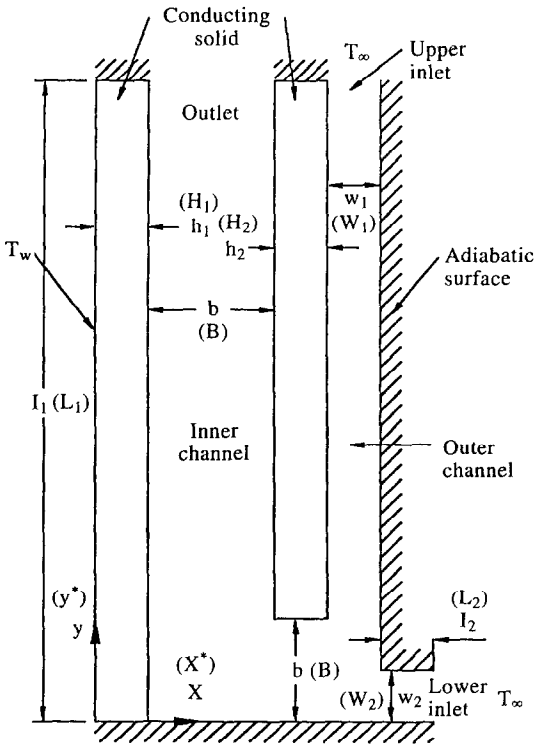

Fig. 1. Schematic diagram of problem geometry.

†Author to whom correspondence should be addressed.

NOMENCLATURE

Ar	inner channel aspect ratio, l_1/b
b	dimensional inner channel width
B	non-dimensional inner channel width, b/b
g_y	acceleration due to gravity
h_1	dimensional left wall thickness
H_1	non-dimensional left wall thickness, h_1/b
h_2	dimensional partition thickness
H_2	non-dimensional partition wall thickness, h_2/b
k	thermal conductivity
K	thermal conductivity ratio, k_w/k_a
l_1	dimensional inner channel height
L_1	non-dimensional inner channel height, l_1/b
l_2	dimensional lower inlet length
L_2	non-dimensional lower inlet length, l_2/b
M	non-dimensional mass flow rate, $M = \dot{m}/\mu b$
p	pressure
p_h	hydrostatic pressure
p_m	motion pressure $(p-p_h)$
Pr	Prandtl number v/α
Ra	Rayleigh number, $g_y\beta(T_w-T_\infty)b^3/\alpha v$
T	temperature
$\mathbf{u}$	velocity vector
U_0	characteristic velocity
W_1	non-dimensional upper inlet width, w_1/b
W_2	non-dimensional lower inlet width, w_2/b
x	Cartesian x coordinate
y	Cartesian y coordinate.

Greek symbols

α	thermal diffusivity
β	coefficient of volumetric expansion
θ	non-dimensional temperature $(T-T_\infty)/(T_w-T_\infty)$
μ	dynamic viscosity
v	kinematic viscosity
ρ	density.

Subscripts

a	working fluid (air) value
i	solid-to-fluid interface value
w	heated wall value
∞	ambient value.

Superscript

*	non-dimensional quantity.

condition (T_w) applied at the left wall external surface. All other external surfaces are considered adiabatic.

Previous studies have looked at a variety of boundary conditions and geometries. A review of the closed and open loop configurations is given by Mertol and Greif [4]. Typically, either isothermal or isoflux boundary conditions are applied. This decouples the flow problem from the conduction problem existing in the walls. Some studies in rather closely related geometries (enclosures and vertical channels) have examined the wall conduction effects [5–7]. These studies lend insight, but do not address the geometry of interest here.

The present work investigates multiple inlets along with wall conduction. A literature review indicates that previous work in this area is limited to one inlet and one outlet [8–10]. The geometry explored in this research essentially combines an 'L' type channel with a 'U' type channel. To the best of our knowledge no information is available in the open literature which studies this configuration.

2. PROBLEM FORMULATION

For the present study the natural convection flow of interest is assumed to be a steady state, two-dimensional, laminar and viscous flow of a constant property fluid. The fluid is Newtonian and incompressible. No heat generation exists in either the fluid or solid regions. Thermal radiative heat transport is neglected. The surroundings consist of an extensive, quiescent, isothermal reservoir at constant temperature T_∞.

The fluid flow and heat transfer are described by the conservation equations for mass (continuity), momentum (Navier–Stokes) and energy. The appropriate equations are expressed in non-dimensional form by using the non-dimensional variables defined below:

$$x^* = \frac{x}{b} \quad y^* = \frac{y}{b} \tag{1}$$

$$\mathbf{u}^* = \frac{\mathbf{u}}{U_0} \quad \theta = \frac{(T-T_\infty)}{(T_w-T_\infty)} \quad p_m^* = \frac{p_m}{\rho U_0^2}. \tag{2}$$

The motion pressure (p_m) is defined as the difference between the actual pressure (p) at any point in the fluid and the hydrostatic pressure (p_h) that would exist at the same point in the absence of fluid flow. It appears as a consequence of the Boussinesq approximation which models the interaction of the body force (gravity) with temperature-induced local density variations.

The characteristic velocity (U_0) is based on equating the kinetic energy per unit volume of the flow to the work input per unit volume by the buoyancy force

acting over the length of the heated wall. It is defined as:

$$U_0 = \frac{\alpha}{b}\sqrt{Ra\,Pr\,Ar}. \tag{3}$$

By substituting these dimensionless quantities into the governing equations for mass, momentum and energy, the normalized governing equations are obtained. Note the buoyancy term (θ/Ar) appears only in the vertical (y) component of equation (5). The resultant equations are as follows for the fluid region:

$$\nabla\cdot\mathbf{u}^* = 0 \tag{4}$$

$$(\mathbf{u}^*\cdot\nabla)\mathbf{u}^* = -\nabla p_m^* + \sqrt{\left(\frac{Pr}{Ra\,Ar}\right)}\nabla^2\mathbf{u}^* + \frac{\theta}{Ar}\mathbf{j} \tag{5}$$

$$(\mathbf{u}^*\cdot\nabla\theta) = \nabla^2\theta\frac{1}{\sqrt{Ra\,Pr\,Ar}} \tag{6}$$

and for the solid regions:

$$\nabla^2\theta = 0. \tag{7}$$

The non-dimensional parameters appearing in the normalized governing equations are the Rayleigh number (Ra), the Prandtl number (Pr) and the inner channel aspect ratio (Ar), where

$$Ra = \frac{g_y\beta(T_w - T_\infty)b^3}{\alpha\nu} \quad Pr = \frac{\nu}{\alpha} \quad Ar = \frac{l_1}{b}. \tag{8}$$

The normalized boundary conditions are given next. Refer to Fig. 1 for dimensioning nomenclature. The thermal boundary conditions include the isothermal external surface of the heated wall ($\theta_w = 1$) and adiabatic conditions at the remaining external surfaces:

$$\theta = \theta_w \quad \text{for } x^* = 0 \quad \text{and} \quad 0 \leqslant y^* \leqslant L_1 \tag{9}$$

$$\frac{\partial\theta}{\partial n^*} = 0 \text{ for}$$

$$\begin{bmatrix} 0 \leqslant x^* \leqslant (H_1+B+H_2+W_1+L_2) \text{ and } y^* = 0 \\ 0 \leqslant x^* \leqslant H_1 \text{ and } y^* = L_1 \\ (H_1+B+H_2+W_1) \leqslant x^* \\ \qquad \leqslant (H_1+B+H_2+W_1+L_2) \text{ and } y^* = W_2 \\ x^* = (H_1+B+H_2+E_1) \text{ and } W_2 \leqslant y^* \leqslant L_1 \\ (H_1+B) \leqslant x^* \leqslant (H_1+B+H_2) \text{ and } y^* = L_1 \end{bmatrix} \tag{10}$$

where (n^*) is the direction normal to the boundary.

Boundary conditions at the inlets are specified so that the inflow is at the reservoir temperature $(\theta = 0)$ and the lateral fluid velocity is also zero. This is shown explicitly below for the upper and lower inlets.

$$\begin{bmatrix} u^* = 0 \\ \theta = 0 \end{bmatrix} \text{for } (H_1+B+H_2) \leqslant x^* \leqslant (H_1+B+H_2+W_1) \text{ and } y^* = L_1 \tag{11}$$

$$\begin{bmatrix} v^* = 0 \\ \theta = 0 \end{bmatrix} \text{for } x^* = (H_1+B+H_2+W_1+L_2)$$

$$\text{and } 0 \leqslant y^* \leqslant W_2. \tag{12}$$

Conditions at the outlet are essentially unknown. Previous works by Abib and Jaluria [11] and Jones and Cai [12] indicate that setting the temperature gradient equal to zero in the vertical direction for outflow at the exit adequately approximates the interaction between the thermosyphon and the surroundings. It is also an acceptable practice that the temperature of inflow is that of the reservoir $(\theta = 0)$. Chan and Tien [13], however, showed that the heat transfer and the flow field are only weakly affected by the state of the inflow.

The outlet thermal boundary condition used here specifies zero vertical temperature gradient all along the outlet; however, simultaneous inflow and outflow at the outlet of the inner channel is expected. This is true particularly at larger Rayleigh numbers as boundary layer flow develops along the heated wall. The findings of Chan and Tien [13] give confidence that this boundary condition is also reasonable for regions of inflow at the outlet as results are affected little. Outlet boundary conditions are given below:

$$\begin{bmatrix} u^* = 0 \\ \dfrac{\partial\theta}{\partial y^*} = 0 \end{bmatrix} \text{for } H_1 \leqslant x^* \leqslant (H_1+B) \text{ and } y^* = L_1. \tag{13}$$

To complete the boundary conditions the velocity at all the wetted surfaces is set equal to zero. It is expressed as

$u^* = v^* = 0$ for

$$\begin{bmatrix} x^* = H_1 \text{ and } 0 \leqslant y^* \leqslant L_1 \\ H_1 \leqslant x^* \leqslant (H_1+B+H_2+W_1+L_2) \\ \qquad \text{and } y^* = 0 \\ (H_1+B+H_2+W_1) \leqslant x^* \\ \qquad \leqslant (H_1+B+H_2+W_1+L_2) \text{ and } y^* = W_2 \\ x^* = (H_1+B+H_2+W_1) \text{ and } W_2 \leqslant y^* \leqslant L_1 \\ x^* = (H_1+B) \text{ and } B \leqslant y^* \leqslant L_1 \\ x^* = (H_1+B+H_2) \text{ and } B \leqslant y^* \leqslant L_1 \\ (H_1+B) \leqslant x^* \leqslant (H_1+B+H_2) \text{ and } y^* = B \end{bmatrix}. \tag{14}$$

One additional condition is imposed on the numerical solution. The fluid-to-solid interface condition is expressed in non-dimensional terms where the thermal conductivity ratio, $K = k_w/k_a$, appears as a consequence of the continuous heat flux across the interface:

$$K\left(\frac{\partial\theta}{\partial n^*}\right)_{\text{solid}} = \left(\frac{\partial\theta}{\partial n^*}\right)_{\text{fluid}}. \tag{15}$$

The continuity of temperature boundary condition at the fluid-to-solid interface is expressed as:

$$\theta_{\text{solid}} = \theta_{\text{fluid}}. \quad (16)$$

The function of the preceding non-dimensional formulation is primarily to identify relevant non-dimensional parameters and not for numerical computations. Note that a proprietary code known as COSMOS/M was used to obtain solutions for the primitive variable form of the governing equations. They are discretized using the Galerkin method of weighted residuals. A four-node quadrilateral element is used with the interpolation functions being bilinear for both temperature and velocity. The pressure variable is eliminated using a penalty function formulation. Converged solutions are obtained using the Newton–Raphson or Picard iteration methods. A detailed description of the code is documented in ref. [14].

3. NUMERICAL INVESTIGATION

Consideration of the normalized governing equations indicates that a parametric study of the flow and temperature fields for the present problem involves the non-dimensional parameters Ra, Ar and Pr. Other geometric parameters (see Fig. 1) which do not appear explicitly in the normalized governing equations but appear in the boundary conditions include the partition width H_2, the inlet channel widths W_1 and W_2, and the lower inlet channel length L_2. A complete investigation including all of these parameters is beyond the scope of this study.

The project was limited first of all by considering only air as the working fluid ($Pr = 0.71$). Other constants are the upper inlet channel width ($W_1 = B/2$), the lower inlet channel length ($L_2 = B/2$), the partition wall thickness ($H_2 = B/2$) and the aspect ratio ($Ar = 6$). To examine the effects of the remaining parameters (Ra, K, W_2) on the flow and temperature fields, each was varied independently of the others over a range of values. The ranges of Ra, K and W_2 investigated for the purpose of the present study were 10^3–10^6, 0.1–10.0 and 0.0–0.75, respectively. A total of 128 cases were run for this purpose. The detailed computational matrix in this regard is presented in ref. [15] and will not be repeated here.

An independent mesh for each value of the lower inlet width (W_2) was constructed. Non-uniform meshes were used to decrease the number of elements required and still resolve areas of high temperature and velocity gradients. Use of non-uniform meshes is based on the idea that dense packing of small elements in regions of high gradients will yield improved accuracy. This is done provided that regions of larger, less dense elements do not degrade the overall accuracy of the solutions.

To test for mesh independency, two different meshes for a given geometry, mesh 'A' and mesh 'B', were constructed. Mesh A contained approximately twice as many nodes as mesh B. Solutions for the largest Rayleigh number (10^6) were obtained for both the meshes. The computed overall heat transfer rate was then compared for the two meshes. The mesh numbers were then increased until satisfactory results were obtained. In general the results agreed well with a maximum of 1.2% difference in the overall heat transfer rate between the two mesh sizes. A detailed description of the mesh independency tests and a sample distribution of mesh elements are documented in ref. [15] and will not be discussed here. Computations were also performed to show mass balance over the computational domain. For the cases checked, the percentage difference between mass flow in and mass flow out was found to be about 5×10^{-5}. Energy balance was checked for selected cases and the results were similar.

4. RESULTS AND DISCUSSION

As discussed earlier, the objective of this work was to investigate the flow and temperature fields of the open loop thermosyphon configuration of interest. In this study, the Rayleigh number (Ra), the thermal conductivity ratio (K) and the lower inlet width (W_2) were varied to understand their effects.

4.1. *Effect of lower inlet width parameter*

The computed isotherms and streamlines for various values of Ra and W_2 are shown in Fig. 2. The Rayleigh number (Ra) is varied by changing the temperature difference across the thermosyphon ($T_w - T_\infty$). Other parameters are fixed with $K = 5$ and $Ar = 6$. Observation of the isotherms [Fig. 2(a)] reveals changes in the temperature field due to changes in Ra and W_2. Several trends are evident, and are described below.

(1) For $Ra \geqslant 10^4$ and $W_2 > 0.25$, the temperature field becomes relatively independent of the lower inlet width (W_2). At the highest Rayleigh number (10^6), little change is apparent for the entire range of W_2 (0.0–0.75). At lower Ra ($< 10^4$) there are significant changes in the temperature field with changing W_2.

(2) As Ra increases, the isotherms become more packed near the heated wall. The isotherm packing is also greater at low Ra ($\leqslant 5 \times 10^4$) with increasing W_2. Such trends result in the an increasingly narrow thermal boundary layer at the heated wall. Consideration of the streamlines [Fig. 2(b)] also shows some definite trends due to changes in Ra and W_2. The most evident trends are described below.

(3) The occurrence of inflow (recirculation) at the outlet is apparent. This is evident due to the streamlines that both begin and end at the outlet. Recirculation clearly tends to increase with Ra and decrease with larger W_2. It can be seen from the figure that increasing W_2 from 0.25 to 0.50 decreases the recirculation. A further increase ($W_2 = 0.75$) has little additional effect.

(4) A velocity boundary layer develops along the heated wall as the Rayleigh number is increased above

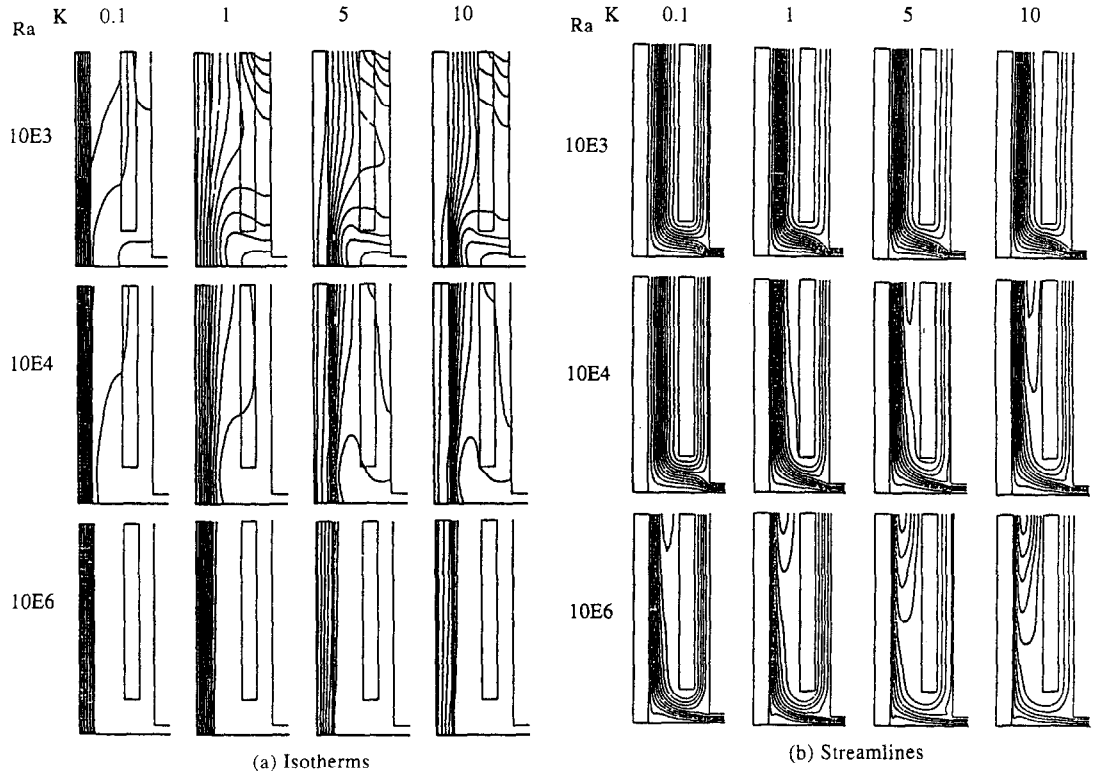

Fig. 2. Plots of the flow field with $K = 5$ and $Ar = 6$ for varying W_2 and Ra.

5×10^4. The boundary layer tends to decrease in thickness with increasing Ra. The effects of W_2 on the velocity boundary layer thickness are not readily apparent.

(5) With the increase of W_2, the inflow at the upper inlet gradually decreases and eventually stops. In that situation all the inflow occurs at the lower inlet and partly at the outlet (recirculation effect).

The observations described in points (1)–(5) are next examined to determine the mechanisms that cause these effects. First, consider (3), the recirculation at the outlet. Figure 2(b) shows that for fixed Ra, decreasing W_2 (< 0.50) tends to increase the recirculation. Thus, if insufficient mass flow is available at the inlets due to flow restrictions, compensating flow will be drawn in from the outlet channel. Recirculation also increases with increasing Rayleigh number. Figure 3 gives some indication why this occurs.

Figure 3(a) shows the normalized total mass inflow rate from all sources including recirculation at the outlet. Figure 3(b) shows the amount of this flow originating at the upper and lower inlets. These figures indicate that the required total mass flow rate increases with increasing values of Ra; however, for restrictive W_2 ($\leqslant 0.25$), inflow at the inlets shows a lower rate of increase. Therefore, at larger Ra the inlets supply an increasingly smaller fraction of the

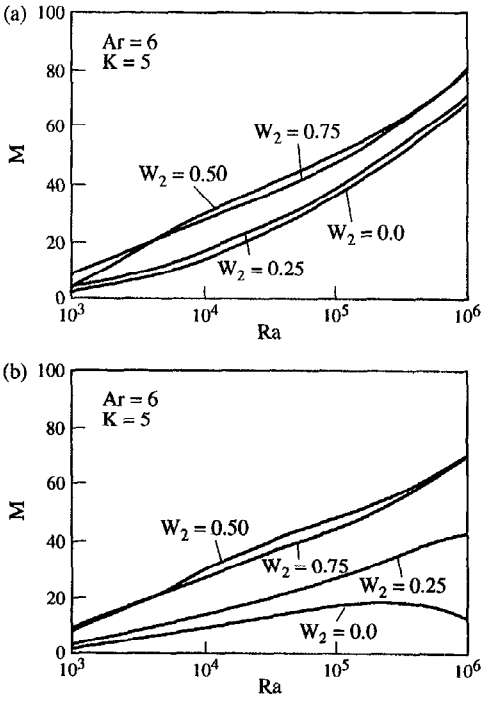

Fig. 3. Mass inflow rate at various values of Ra.

total mass flow and as such recirculation compensates.

Figure 3(b) shows another interesting characteristic. The graph for $W_2 = 0.0$ has an inflection point at approximately $Ra = 3 \times 10^5$. Beyond this point, inlet flow actually decreases while the total mass flow requirement [Fig. 3(a)] continues to increase. This indicates recirculation is becoming dominant and the effects of restricted flow passages at the inlets are compensated by increased inflow from the outlet by recirculation. The other reason for the occurrence of recirculation is the decreased thickness of the boundary layers along the hot wall with increasing Ra. This essentially makes more area at the inner channel (outlet) available for inflow. This trend is discussed further later.

Let us now discuss observation (2), the isotherm movement and developing thermal boundary layer. Examination of the normalized energy equation (6) indicates that as Ra increases the conduction terms become less important and the convection terms become dominant. Thus, convection effects decrease the thermal penetration due to conduction from the heated wall. This effectively reduces the thermal boundary layer thickness. This effect is evident in the isotherm plots and is further detailed in Fig. 4 in which the normalized temperature profile across the outlet is plotted.

Figure 4(a) indicates that decreasing W_2 to 0.25 or less causes increased temperature penetration primarily at low Ra ($< 5 \times 10^4$). This is due to the increased flow restriction at the inlets which reduces inflow and therefore reduces convection effects. This increases conduction effects so that temperature penetration is greater. On the other hand, Fig. 4(c) and (d) show that at higher values of Ra, thermal penetration due to conduction from the hot wall is greatly reduced because of the increased convection effects.

The thermal boundary layer behavior is important in understanding the recirculation at the outlet. At low values of Ra, elevated temperatures ($\theta = 0.2$ or more) extend well across the outlet of the left channel. As Ra is increased, the thermal boundary layer approaches the wall. This creates a situation where the fluid closer to the partition wall of the inner channel is at a lower temperature (closer to ambient temperature). This temperature can be observed from the isotherm plots of Fig. 2(a). Fluid in this region is drawn towards the vertical hot wall just like the fluid from the inlets of the right channel. Thus, the outlet partially becomes an inlet. This behavior is detailed in Fig. 5 which plots the normalized vertical velocity profile across the outlet.

Figure 5 also shows that the vertical velocity increases with increasing Ra. This is because increasing Ra essentially increases the temperature difference $(T_w - T_\infty)$ across the thermosyphon. This increases the solid-to-fluid interface temperature which imparts a larger thermal buoyancy force to the fluid. Thus, a larger vertical velocity results. This is the reason for the observed velocity boundary layer development, as discussed in point (4) earlier. The negative values of vertical velocities in Fig. 5 are indicative of recirculation flows. It can be seen that with increasing values of Ra, the width of the recirculating flow area at the channel outlet increases.

It is useful at this point to discuss the flow restrictions. For the present problem, the partition wall, the inlet channels and associated boundaries all serve to restrict fluid inflow. Various mechanisms cause the flow restrictions. Flow restriction at the inlets is in large part due to viscous losses. These depend among other things on the inlet channels' lengths and widths. Another obvious effect of the partition and inlet configuration is that the reservoir fluid has limited physical access to the heated wall.

The conducting partition wall complicates the flow by introducing temperature-dependent flow conditions at the upper inlet channel. If the partition wall were adiabatic, flow inside the upper inlet channel would be isothermal due to pressure gradients. With a conducting partition, however, thermal buoyancy forces oppose the flow.

Buoyancy forces in the upper inlet channel are due to heat energy transferred across the partition originating at the left vertical heated wall. Heat transfer from the heated wall to the partition (across the inner channel) is by conduction in the fluid as there is no fluid velocity in this direction. Thus, flow restriction due to the partition heat transfer is expected to decrease with increasing Ra. This is because of the fact that with higher Ra, the conduction heat transfer across the inner channel is reduced. As such the partition wall is at a lower temperature, therefore there is less effect of the opposing buoyancy forces at the upper inlet. Thus, the heat transfer through the partition decreases significantly with increasing Ra. In this study the flow restriction due to opposing thermal buoyancy forces is found to be negligible and essentially independent of W_2 for Ra greater than 5×10^4.

Reasons for observation (1), reported earlier, that the temperature field is independent of W_2 for $Ra \geqslant 10^4$, are now evident. With increasing Rayleigh number, heat transfer in the fluid is dominated by convection, and a thermal boundary layer develops. This has two primary results: cool reservoir fluid has greater access to the heated wall via the outlet (recirculation); and opposing buoyancy effects in the upper inlet decrease and as such improve access there. Access is improved sufficiently to compensate for any flow reduction due to the inlet configuration and lower values of W_2.

4.2. *Effect of thermal conductivity parameter*

The computed isotherms and stream functions for various values of Ra and K are shown in Fig. 6. The other parameters are fixed with $W_2 = 0.25$ and $Ar = 6$. The isotherm plots [Fig. 6(a)] are examined first for characteristic trends. The trends will

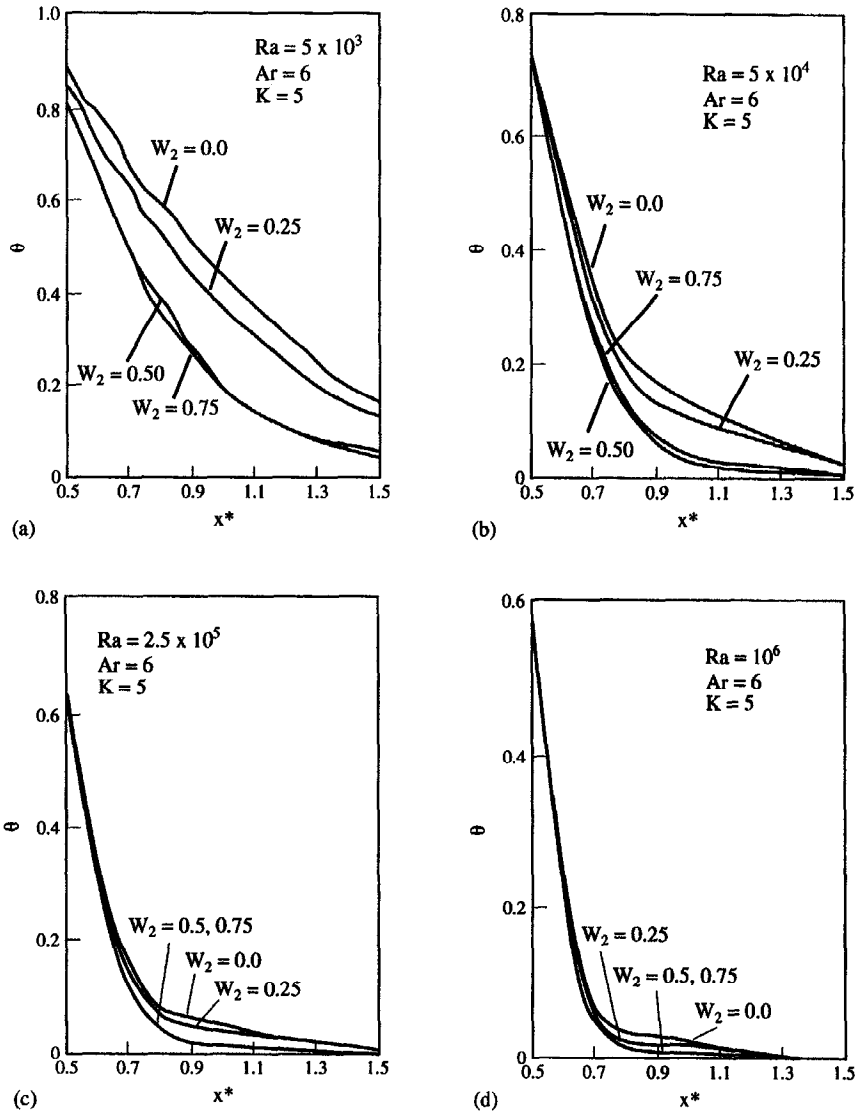

Fig. 4. Temperature distribution across outlet with different values of W_2 and Ra.

be described and examined later to determine causes.

(1) The most obvious trend occurs in the heated wall where the temperature gradients across the wall increase with reduced values of K. This is most evident for K values less than five.

(2) In the region extending from approximately the middle of the inner channel up to the outer channel boundary wall, the temperature field does not change dramatically for a given value of Ra as K increases. This characteristic appears to be true regardless of the Rayleigh number magnitude. The exception to this trend is at $K = 0.1$ where most of the temperature drop is across the wall.

(3) It is also evident that a thermal boundary layer develops with increasing Ra. It appears that for a given Ra, increasing the value of K accelerates this effect.

Observation of Fig. 6(b), the stream function plots, also reveals some clear trends. These are described below.

(4) Recirculation at the outlet tends to increase with the increase in values for both the parameters Ra and K. Note that with the restrictive lower inlet width ($W_2 = 0.25$) a significant portion of the total mass flow enters at the upper inlet for each case.

(5) It is clear that a velocity boundary layer develops as Ra increases. This boundary layer also develops more readily for larger K values.

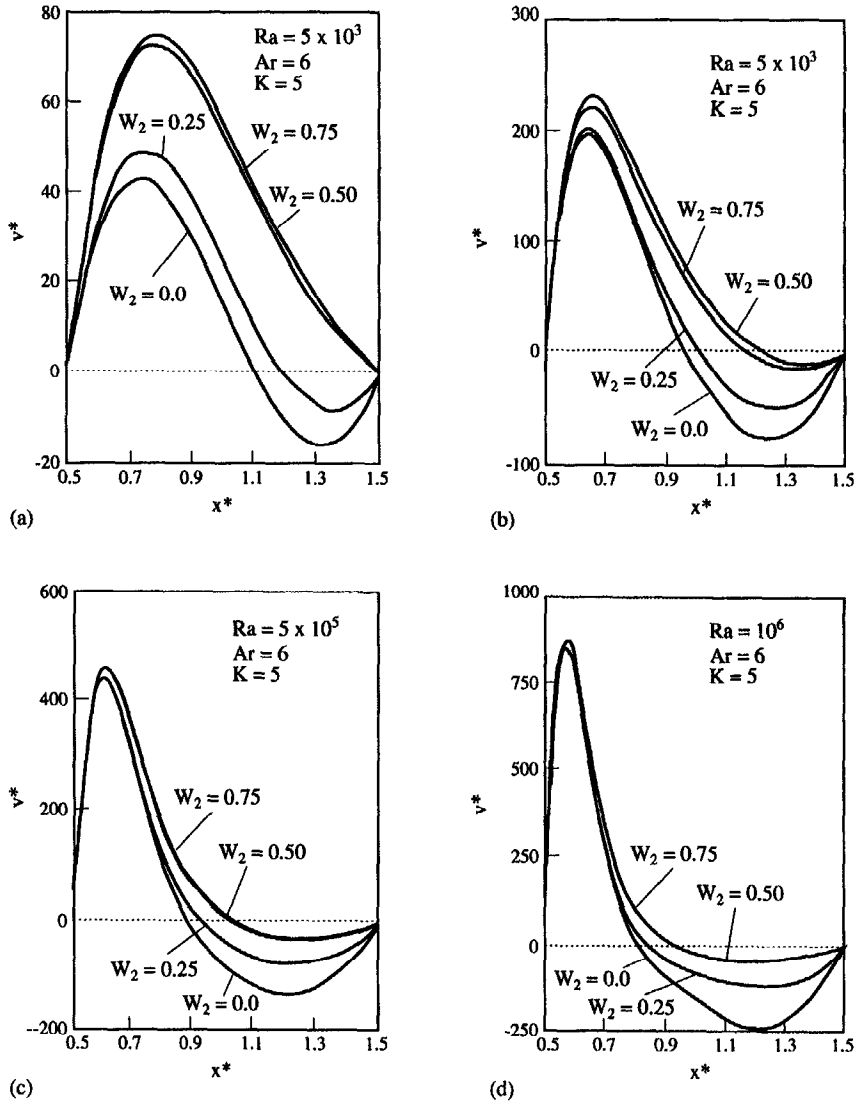

Fig. 5. Vertical velocity distribution across outlet with different values of W_2 and Ra.

The characteristics described above are next examined to determine the causes for the observed behavior. Let us first consider observation (1), the heated wall temperature gradients. The temperature gradients across the wall are due to wall thermal conductivity and convection at the wall surface. Both of these are affected strongly by the values of K. With lower values of K, the conductive resistance across the wall increases, hence higher temperature gradients there. It can also be seen from Fig. 6(a) that at higher values of Ra, and with $K = 0.1$, the temperature gradients exist only in a solid hot wall. The fluid in the channel is essentially isothermal.

Next examine observation (4), the recirculation tendency which increases with the increase of both Ra and K values. As shown previously, the recirculation is due to restricted inflow and is increased by the formation of thermal and velocity boundary layers. As the boundary layers develop, more area of the outlet is available for fluid inflow. Thus, anything that promotes boundary layer development will promote recirculation.

Increasing the values of K reduces the wall conduction resistance and effectively increases the wall-to-fluid interface temperature. Increasing Ra has a similar effect because larger Ra essentially means $(T_w - T_\infty)$ is increased. Figure 7 details this effect. To interpret Fig. 7 properly, note that the non-dimensional temperature (θ) always lies between zero and unity for all Rayleigh numbers. However, the relative magnitude of the actual physical temperature difference $(T - T_\infty)$ varies as follows:

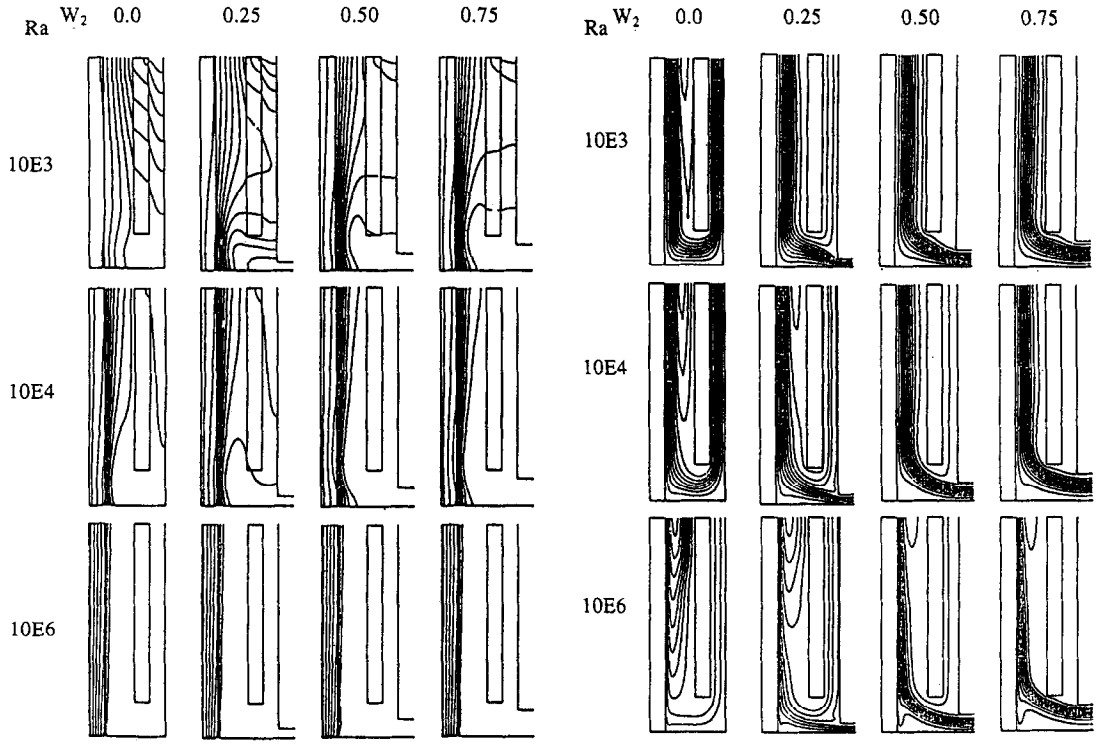

(a) Isotherms (b) Streamlines

Fig. 6. Plots of the flow field with $W_2 = 0.25$ and $Ar = 6$ for varying K and Ra.

$$(T - T_\infty) = Ra\,\theta \frac{\alpha \nu}{g_y \beta b^3}. \quad (17)$$

For constant fluid properties, the physical temperature difference magnitude is proportional to the product of Ra and θ. Thus, while Fig. 7 shows the non-dimensional temperature θ_i decreases with increasing Ra, the actual physical solid-to-fluid interface temperature is increasing.

Increasing the solid-to-fluid interface temperature promotes boundary layer development because it imparts a larger thermal buoyancy force to the fluid. This results in a greater vertical velocity near the wall and a reduction in the thermal and velocity boundary layer thicknesses. This trend was reported earlier in observations (3) and (5).

Near and within the heated wall, K has a large influence on the temperature field. It has much less influence further from the wall [observation (2)]. This is explained simply by noting that much of the temperature drop occurs across the wall or across the thermal boundary layer. Increasing K reduces the temperature drop across the wall. This sharply increases the temperature drop across the thermal boundary layer because θ_i is greater. In contrast, decreasing K magnifies the wall temperature drop and reduces the boundary layer drop. The net effect is that for a constant Rayleigh number the temperature field further from the heated wall is less affected by the change in K values. This is because much of the temperature drop occurs across the heated wall or inside the thermal boundary layer.

5. CONCLUSIONS

The velocity and temperature fields resulting from an isothermally heated wall-driven flow have been investigated for the thermosyphon with two inlets and conducting walls. The results indicate that the temperature field becomes independent of the lower inlet configuration for $Ra > 10^4$; however, the flow field is very much affected by the lower inlet width. Recirculation at the outlet tends to compensate for flow restriction at the inlets. Recirculation increases with both Ra and K due to formation of the thermal boundary layer resulting in increased access for cool reservoir fluid via the outlet. Recirculation eventually becomes dominant as Ra is increased for restrictive lower inlet widths.

For $Ra \leqslant 10^4$ and restrictive lower inlet widths ($W_2 < 0.50$) the temperature field shows increased conduction effects as the isotherms penetrate further from the heated wall. Inlet flow restrictions inhibit convection and thus increase conduction effects. Low wall conductivity results in large temperature gradients across the heated wall and reduction in convection at the wall surface. The temperature field further from the heated wall is slightly affected by the change in K values as much of the temperature drop

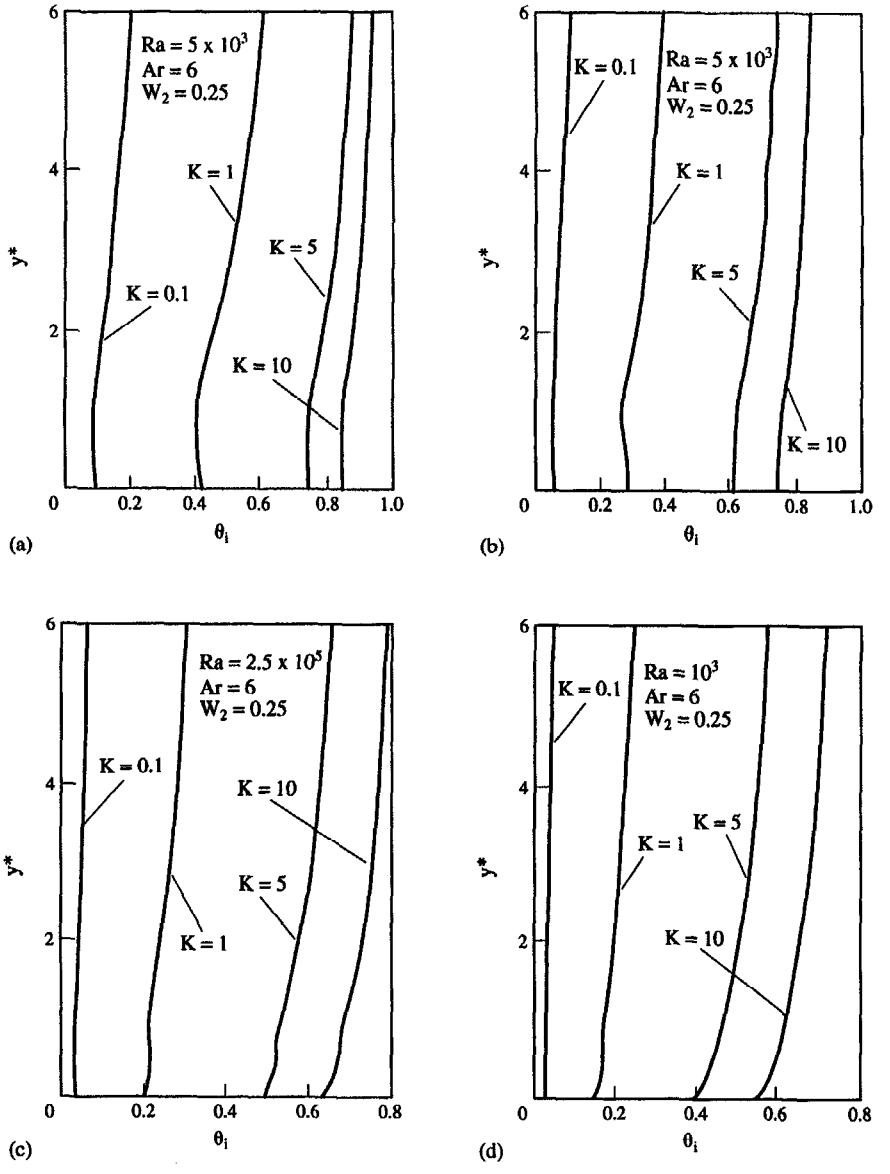

Fig. 7. Heated wall and fluid interface temperature distribution with parameters K and Ra.

occurs across the heated wall or the inside of the thermal boundary layer.

REFERENCES

1. R. Clarksean, Experimental analysis of natural convection within a thermosyphon, *The Third World Conference on Experimental Heat Transfer, Fluid Mechanics, and Thermodynamics*. Honolulu, Hawaii (1993).
2. W. Kwant and C. E. Boardman, PRISM-Liquid metal cooled reactor plant design and performance, *Nucl. Engng Des.* **136**, 111–120 (1992).
3. K. E. Torrance, Open loop thermosyphons with geological applications, *J. Heat Transfer* **101**, 677–683 (1979).
4. A. Mertol and R. Greif, A review of natural circulation loops. In *Natural Convection Fundamentals and Applications* (Edited by S. Kakac, W. Aung and R. Viskanta). Hemisphere, Washington, DC (1985).
5. T. Burch, T. Rhodes and S. Acharya, Laminar natural convection between finitely conducting vertical plates, *Int. J. Heat Mass Transfer* **28**, 1173–1186 (1985).
6. D. A. Kaminski and C. Prakash, Conjugate natural convection in a square enclosure: effect of conduction in one of the vertical walls, *Int. J. Heat Mass Transfer* **29**, 1979–1988 (1986).
7. S. H. Kim, N. K. Anand and W. Aung, Effect of wall conduction on free convection between asymmetrically heated vertical plates: uniform wall heat flux, *Int. J. Heat Mass Transfer* **33**, 1013–1023 (1990).
8. Y. D. Lapin, Heat transfer in communicating channels under conditions of free convection, *Thermal Engng* **16**, 94–97 (1969).
9. K. E. Torrance and V. W. C. Chan, Heat transfer by a free convection loop embedded in a heat-conducting solid, *Int. J. Heat Mass Transfer* **23**, 1091–1097 (1980).
10. H. H. Bau and K. E. Torrance, Transient and steady behavior of an open, symmetrically-heated, free convection loop, *Int. J. Heat Mass Transfer* **24**, 597–609 (1981).

11. A. H. Abib and Y. Jaluria, Numerical simulation of the buoyancy-induced flow in a partially open enclosure, *Numer. Heat Transfer* **14,** 235–254 (1988).
12. G. F. Jones and J. Cai, Analysis of a transient asymmetrically heated/cooled open thermosyphon, *J. Heat Transfer* **115,** 621–630 (1993).
13. Y. L. Chan and C. L. Tien, A numerical study of two-dimensional laminar natural convection in shallow open cavities, *Int. J. Heat Mass Transfer* **28,** 603–612 (1985).
14. COSMOS/M Users Manual, Version 1.70, Structural Research and Analysis Corporation, Santa Monica, CA (1993).
15. J. J. Fleming, Conjugate natural convection heat transfer in a planar thermosyphon with multiple inlets, M. S. Thesis, Montana State University, Bozeman, MT (1994).